

NUMERICAL STUDY OF THE AMICK-SCHONBEK SYSTEM IN 2D

CHRISTIAN KLEIN AND JEAN-CLAUDE SAUT

This paper is dedicated to the memory of Vladimir E. Zakharov

ABSTRACT. A numerical study of the 2D Amick-Schonbek Boussinesq system is presented. Numerical evidence is given for the transverse stability of the 1D solitary waves that are line solitary waves of the 2D equations. It is shown that initial data not satisfying the non-cavitation condition can lead to the formation of a gradient catastrophe in finite time. The numerical propagation of localised smooth initial data does not lead to the formation of stable structures localised in both spatial directions. For initial data satisfying the non-cavitation condition, smooth solutions appear to exist for all times.

1. INTRODUCTION

This paper presents numerical simulations of a special case of two-dimensional Boussinesq systems for the propagation of long, weakly nonlinear waves in the so-called Boussinesq regime. Those systems degenerate to the Korteweg-de Vries equation when restricted to one-dimensional, one way propagating waves. They model water waves on a flat bottom propagating in both directions in the aforementioned regime (see [8, 9, 10]). The rigorous derivation is obtained by expanding the Dirichlet to Neumann operator occurring in the Zakharov-Craig-Sulem formulation of the water waves system [47, 16] with respect to the small parameter ϵ (see below).

1.1. Background. More precisely we will consider a particular case of the so-called abcd Boussinesq systems for surface water waves, see [8, 9, 10]. Note that Boussinesq [11] was the first to derive particular Boussinesq systems, but not in the class of those studied here. We refer to [17, 18, 19] for details and the history of hydrodynamics in the nineteenth century. The systems can be put into the form

$$(1.1) \quad \begin{cases} \eta_t + \nabla \cdot \mathbf{v} + \epsilon \nabla \cdot (\eta \mathbf{v}) + \mu [a \nabla \cdot \Delta \mathbf{v} - b \Delta \eta_t] = 0 \\ \mathbf{v}_t + \nabla \eta + \epsilon \frac{1}{2} \nabla |\mathbf{v}|^2 + \mu [c \nabla \Delta \eta - d \Delta \mathbf{v}_t] = 0. \end{cases}$$

Here $\eta = \eta(x, t)$, $x \in \mathbb{R}^d$, $d = 1, 2$, $t \in \mathbb{R}$ is the elevation of the wave, $\mathbf{v} = \mathbf{v}(x, t)$ is a measure of the horizontal velocity, μ and ϵ are the small parameters (shallowness and nonlinearity parameters respectively) defined as

$$\mu = \frac{h^2}{\lambda^2}, \quad \epsilon = \frac{\alpha}{h}$$

where α is a typical amplitude of the wave, h a typical depth and λ a typical horizontal wavelength.

Date: January 22, 2025.

In the Boussinesq regime, ϵ and μ are supposed to be small and of same order, $\epsilon \sim \mu \ll 1$. For simplicity we will put $\epsilon = \mu$, writing (1.1) as

$$(1.2) \quad \begin{cases} \eta_t + \nabla \cdot \mathbf{v} + \epsilon[\nabla \cdot (\eta \mathbf{v}) + a \nabla \cdot \Delta \mathbf{v} - b \Delta \eta_t] = 0 \\ \mathbf{v}_t + \nabla \eta + \epsilon[\frac{1}{2} \nabla |\mathbf{v}|^2 + c \nabla \Delta \eta - d \Delta \mathbf{v}_t] = 0. \end{cases}$$

Particular cases are formally derived in [12, 20, 39], see also [20]. The coefficients (a, b, c, d) are restricted by the condition

$$a + b + c + d = \frac{1}{3} - \tau,$$

where $\tau \geq 0$ is the surface tension coefficient.

All (well-posed) members of the abcd class provide the same approximation of the water wave system in the Boussinesq regime, with an error of order $O(\epsilon^2 t)$ (see [8]), and their dispersion relations are similar in the long wave regime. Nevertheless they possess rather different mathematical properties as nonlinear dispersive systems due to the different behavior of the dispersion relation at high frequencies. In fact the order of their dispersive part can vary from +3 to -1, [9, 10]. We refer to [36] for a careful analysis of linear dispersive estimates for the abcd systems.

Two particular one-dimensional cases of the abcd systems have remarkable properties and were studied numerically in [31, 32]. We focus here on the two-dimensional version of one of them. This system is a particular case of a system derived by Peregrine in [39], and it is often referred to as the Peregrine or classical Boussinesq system, but Schonbek and Amick were the first to recognize its remarkable mathematical properties. A variant with slowly varying bottom is derived in [45, 46]. This particular case corresponds to $a = b = c = 0$, $d = 1$ and thus

$$(1.3) \quad \begin{cases} \eta_t + v_x + \epsilon(\eta v)_x = 0 \\ v_t + \eta_x + \epsilon(v v_x - v_{xxt}) = 0. \end{cases}$$

which can be seen as the BBM regularization of a (linearly ill-posed) system obtained from the Zakharov-Craig-Sulem formulation of the water wave system after expanding the Dirichlet-to-Neumann operator at first order in ϵ .

It turns out that the hyperbolic structure of the underlying Saint-Venant (Shallow Water) system can be used for solving the Cauchy problem of the one-dimensional Amick-Schonbek system. In particular the entropy of the Saint-Venant system helps to derive an a priori bound for the solutions of the Amick-Schonbek system, leading to the global well-posedness of the Cauchy problem for arbitrary large initial data satisfying the physical non-cavitation condition, see [2, 42] and [38], this last paper presenting the sharpest results, in particular the existence of global weak solutions. Note that the large time behavior of these solutions is not known. We refer to [31] for numerical simulations leading to relevant conjectures.

There have been many papers dealing with the numerical study of the one-dimensional Amick-Schonbek system, see for instance [3, 4, 31]. The case of a non-flat bottom is considered in [27] and the periodic case in [5]. Solitary waves were constructed in [15], where their interaction was also studied.

The present paper is a continuation of a previous work [31] that considered the 1D case. We focus here on the two-dimensional case for which the existence (and asymptotic behavior) of global solutions is still an open issue both for small and large initial data and thus for which numerical simulations are crucial to present relevant conjectures.

The two-dimensional Amick-Schonbek system writes (we have kept the small parameter ϵ):

$$(1.4) \quad \begin{cases} \eta_t + \nabla \cdot \mathbf{v} + \epsilon[\nabla \cdot (\eta \mathbf{v})] = 0 \\ \mathbf{v}_t + \nabla \eta + \epsilon[\frac{1}{2} \nabla |\mathbf{v}|^2 - d\Delta \mathbf{v}_t] = 0. \end{cases}$$

We are not aware of a connection between (1.4) and the hyperbolic structure the underlying two-dimensional Saint-Venant system similar to the aforementioned results of the 1D case leading for instance to the global existence of weak solutions. The local well-posedness of the Cauchy problem is relatively standard, (see [10] in the 1D case but the extension to the 2D case is straightforward). The existence on long times of order $O(1/\epsilon)$ of solutions to the Cauchy problem for (1.4) that is needed for the full rigorous justification of the system, see [8], was established in [41], Theorem 4.4, under the non-cavitation condition $1 + \eta_0 \geq H_0 > 0$ and in [13] without this condition.

Remark 1.1. The long time existence for a two-dimensional Amick-Schonbek system in presence of a non-trivial bathymetry is proven in [37].

On the other hand, as aforementioned, the *global* behavior of solutions to the 2D Amick-Schonbek system is unknown. In particular the possibility of finite-time blow-up for solutions with initial data satisfying the non-cavitation condition is an open question. The aim of the present paper is to present numerical simulations leading to relevant conjectures, on the qualitative properties of solutions of the Cauchy problem.

1.2. Main results. In this paper we first study for the 1D solitary waves the stability which was also considered in the 1D setting in [31]. Obviously these 1D solutions are infinitely extended (in y) solutions to the 2D system (1.4), so-called line solitary waves. We consider numerically 2D perturbations of these line solitary waves and present evidence for the following

Conjecture 1.1. The line solitary waves of the Amick-Schonbek system are asymptotically stable.

Initial data not satisfying the non-cavitation condition were studied in 1D numerically in [31]. We expand on these results and consider initial data violating this condition in one point in the 2D case. This leads to the following

Conjecture 1.2. Initial data violating the non-cavitation condition in one point in 1D lead to a gradient catastrophe in finite time.

Similar results appear to hold in 2D, but we do not have access to sufficient numerical resolution in this case to present as convincing evidence as in the 1D case.

We study the time evolution of 2D localised initial data and show that it forms an annular structure which then leads to a similar dynamical behavior as initial data that come close to violating the non-cavitation condition. In particular we do not find lump solutions to this system as known from the Kadomtsev-Petviashvili (KP) I equation. It appears that solutions to the 2D system show a similar behavior as solutions to the KP II equation. The Boussinesq equation appears to have a *defocusing* effect. We get the following

Conjecture 1.3. Localised smooth initial data satisfying the non-cavitation condition do not lead to stable structures localised in both spatial dimension. The solutions exist for all times and are simply dispersed.

Furthermore we study the appearance of zones of rapid modulated oscillations in the vicinity of shocks of the solutions to the same initial data for the corresponding Saint-Venant system, so called *dispersive shock waves* (DSWs).

This paper is organized as follows. In section 2 we discuss the transverse stability of line solitary waves. Section 3 is devoted to the behavior of solutions corresponding to initial data violating the non-cavitation condition. In section 4 the time evolution of 2D localised smooth initial data is studied. Section 5 is focussed on dispersive shock waves arising in the zero dispersion limit. We add some concluding remarks in section 6.

2. TRANSVERSE STABILITY OF LINE SOLITARY WAVES

The solitary waves constructed numerically for the 1D AS system, see for instance [31] and references therein, are y -independent traveling wave solutions to the 2D AS system (1.4). These solitary waves infinitely extended in y -direction form so-called line solitary waves. In this section we will study the transverse stability of these waves, i.e., their stability under small perturbations with a non-trivial y -dependence. We will present numerical evidence for the transverse stability of the line solitary waves.

2.1. Numerical approach. The numerical approach to be applied in this paper is essentially a 2D version of the 1D code in [31]. For the spatial coordinates we use a discrete Fourier transform which is conveniently computed with a 2D fast Fourier transform (FFT). This means we approximate a setting in \mathbb{R}^2 by a setting in \mathbb{T}^2 where the torus is chosen to be sufficiently large in both directions that the effects of periodicity are not dominant. In other words the period $2\pi L_x$, $L_x > 0$ is large enough that the reentering radiation is small compared to the effects we want to study. On the other hand the period $2\pi L_y$ in y -direction is small meaning that we essentially consider line solitary waves on \mathbb{T}_y , but we expect that this will not affect the result (for the cases we studied, no effect of the choice of L_y was noted).

In other words we use the standard discretisation $x_n = -\pi L_x + n2\pi L_x/N_x$, $n = 1, \dots, N_x$ and $y_m = -\pi L_y + m2\pi L_y/N_y$, $m = 1, \dots, N_y$. For the time integration of the resulting ODE system for (1.4) we use as in [31] the classical explicit 4th order Runge-Kutta method. The code is tested for the example of the line solitary waves that are propagated to essentially the precision with which they were constructed in [31] if the initial data are unperturbed.

2.2. Perturbed line solitary wave with $c = 2$. The 1D solitary wave solutions $Q_c(x)$ exist for $|c| > 1$, the amplitude of the waves tending to the trivial solution for $|c| \rightarrow 1$. We consider here only positive values of c , i.e., waves traveling to the right. First we consider the case $c = 2$ with $N_x = 2^{12}$ Fourier modes for $x \in 10[-\pi, \pi]$ and $N_y = 2^7$ Fourier modes for $y \in 3[-\pi, \pi]$ with $N_t = 10^4$ time steps for $t \leq 20$. The first perturbation we will look at is of the form

$$(2.1) \quad \eta(x, y, 0) = Q_2(x) \pm 0.3 \exp(-x^2 - y^2), \quad v_x(x, y, 0) = V_2(x), \quad v_y(x, y, 0) = 0..$$

This corresponds to perturbations of the line solitary wave of the order of 5%. Note that we need some finite perturbations to numerically see an effect of the perturbation in finite time.

The solution η for the initial data with the + sign can be seen in Fig. 1 for $t = 0$ and $t = 20$. It appears that the final state corresponds to a line solitary wave with slightly larger velocity $c > 2$ plus radiation.

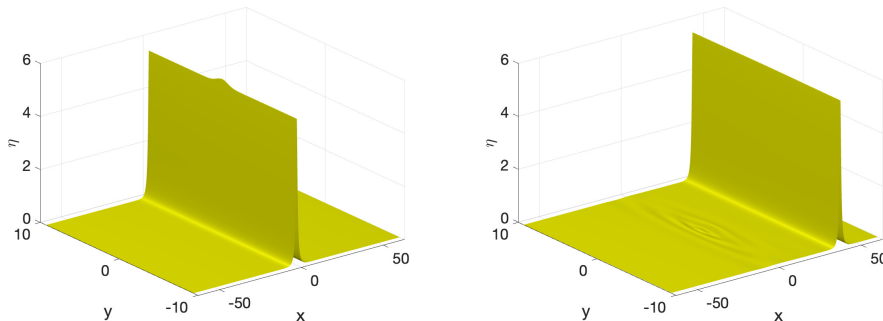


FIGURE 1. Solution to the AS system (1.4) for the initial data (2.1) for the + sign, on the left η for $t = 0$, on the right for $t = 20$.

This interpretation is confirmed by the velocities v_x and v_y which are shown for the same initial data for $t = 20$ in Fig. 2.

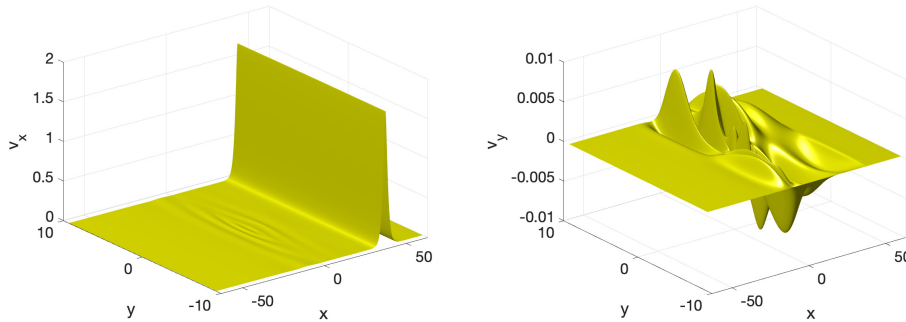


FIGURE 2. Solution to the AS system (1.4) for the initial data (2.1) for $t = 20$, on the left v_x , on the right v_y .

The L^∞ norm of the solution η in this case on the left of Fig. 3 shows oscillations around what appears to be a constant final state, a line solitary wave. The above figures are very similar for the $-$ sign in (2.1). Therefore we only show the L^∞ norm of η in this case on the right of Fig. 3. The final state is reached more slowly, but it appears to be again a line solitary wave, this time with slightly smaller velocity than the unperturbed case with $c = 2$.

If we perturb the velocity v_x by a small Gaussian, i.e., if we consider initial data of the form

$$(2.2) \quad \eta(x, y, 0) = Q_2(x), \quad v_x(x, y, 0) = V_2(x) + 0.1 \exp(-x^2 - y^2), \quad v_y(x, y, 0) = 0,$$

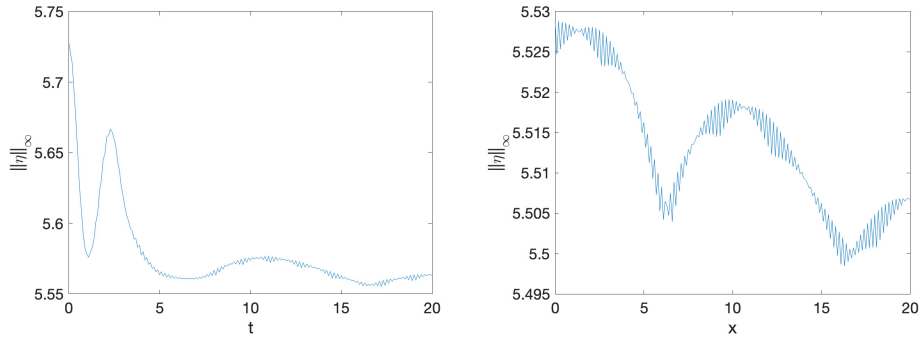


FIGURE 3. L^∞ norm of the solution η to the AS system (1.4) for the initial data (2.1), on the left for the + sign, on the right for the - sign.

we get the solution shown in Fig. 4. Again the final state appears to be a line solitary wave plus radiation.

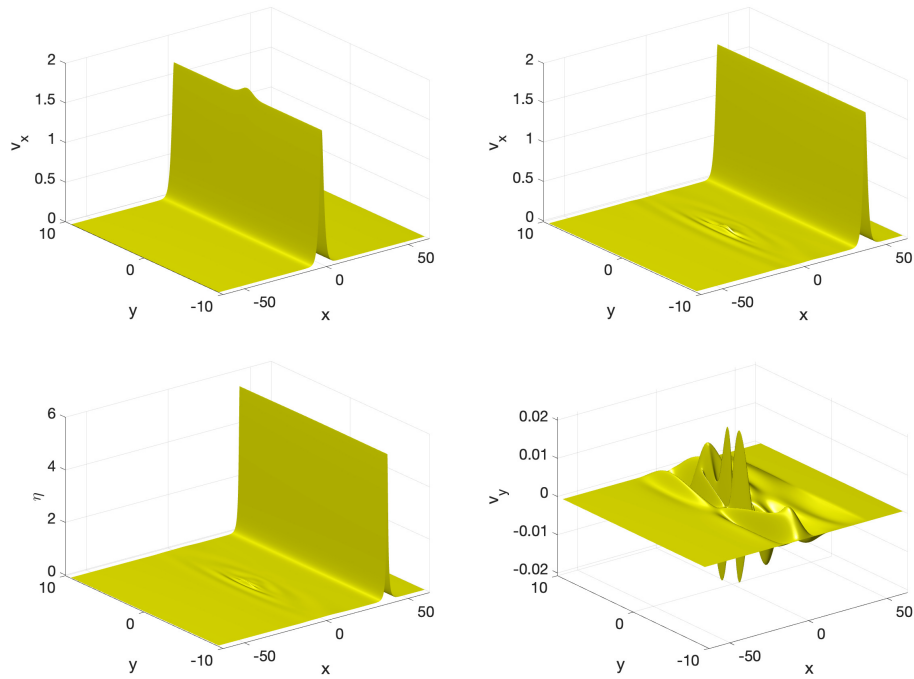


FIGURE 4. Solution to the AS system (1.4) for the initial data (2.2), in the upper row on the left v_x for $t = 0$, on the right for $t = 20$, in the lower row on the left η and on the right v_y , both for $t=20$.

The L^∞ norm of the solution η in Fig. 4 can be seen on the left of Fig. 5. It appears to oscillate around a final state corresponding to a line solitary wave.

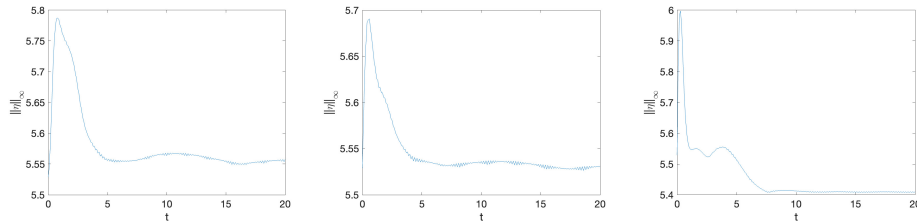


FIGURE 5. L^∞ norms of solutions η to the AS system (1.4) for various initial data, on the left for the solution shown in Fig. 4, in the middle for the solution shown in Fig. 6, on the right for the solution shown in Fig. 8.

If we perturb v_y with a small Gaussian, i.e., if we consider initial data of the form

$$(2.3) \quad \eta(x, y, 0) = Q_2(x), \quad v_x(x, y, 0) = V_2(x), \quad v_y(x, y, 0) = 0.1 \exp(-x^2 - y^2),$$

we get the solution shown in Fig. 6. Once more the final state of the solution seems to be a line solitary wave plus radiation. The L^∞ norm of the solution η in this case can be seen in the middle of Fig. 5. It confirms the interpretation of the final state being a line solitary wave plus radiation.

A different kind of perturbation is to deform the line solitary wave periodically. Concretely we consider initial data of the form

$$(2.4) \quad \eta(x, y, 0) = Q_2(x + 0.4 \cos(y)), \quad v_x(x, y, 0) = V_2(x), \quad v_y(x, y, 0) = 0.$$

The initial condition for η can be seen on the left of Fig. 7. The deformed solitary wave emits some radiation and appears to reach another solitary wave as a final state as suggested by the figure on the right of Fig. 7 for $t = 20$.

This is confirmed by the velocities at the final time $t = 20$ shown in Fig. 8. The L^∞ norm of η in the same figure appears to approach rapidly the final state as can be seen on the right of Fig. 5.

2.3. Perturbed line solitary wave with $c = 1.1$. As an example of solitary waves with velocities close to the threshold $c = 1$, i.e., small slow solitary waves, we consider the case $c = 1.1$. For the numerical experiments we use $N_x = 2^{14}$ Fourier modes for $x \in 40[-\pi, \pi]$ and $N_y = 2^7$ Fourier modes for $y \in 3[-\pi, \pi]$ with $N_t = 2 * 10^4$ time steps for $t < 100$. We consider again localised perturbations with initial data of the form ($\kappa > 0$, $\alpha > 0$)

$$(2.5) \quad \eta(x, y, 0) = Q_{1.1}(x) + 0.01 \exp(-x^2 - \alpha y^2), \quad v_x(x, y, 0) = V_{1.1}(x), \quad v_y(x, y, 0) = 0.$$

This means the perturbation has a maximum of the order of 5% of the wave crest. The initial data for η and the solution for $t = 20$ are shown in Fig. 9. It can be seen that the final state appears to be a line solitary wave of slightly different velocity as in the case for $c = 2$.

The plots for the velocities v_x and v_y are presented in Fig. 10. Once more the final state appears to be a line solitary wave plus radiation.

This interpretation is confirmed by the L^∞ norm of η shown on the left of Fig. 11. It appears to settle on a constant level for larger t indicating that the final state

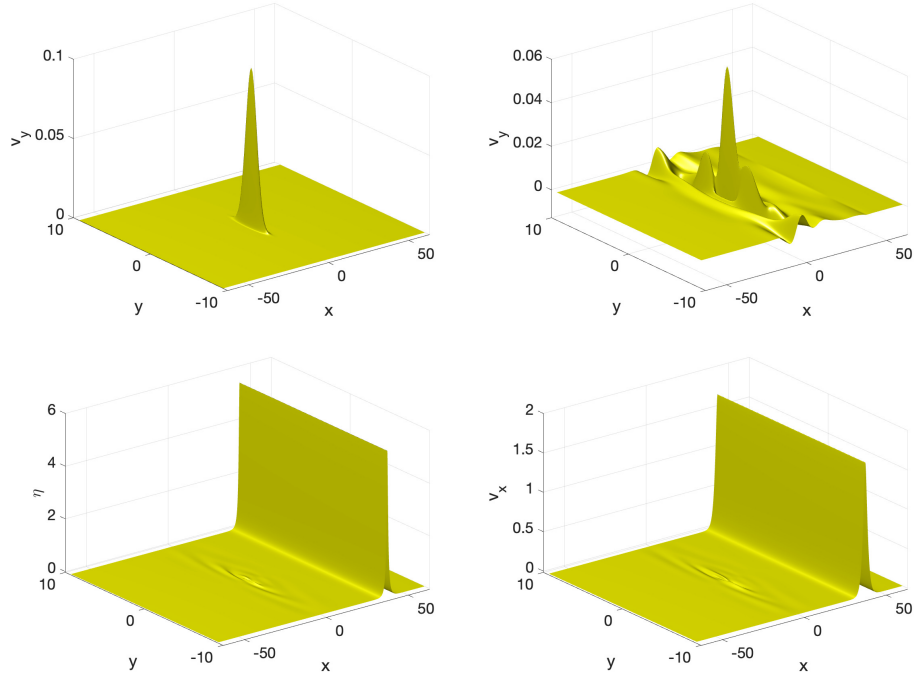


FIGURE 6. Solution to the AS system (1.4) for the initial data (2.4), in the upper row on the left v_y for $t = 0$, on the right for $t = 20$, in the lower row on the left η and on the right v_x , both for $t=20$.

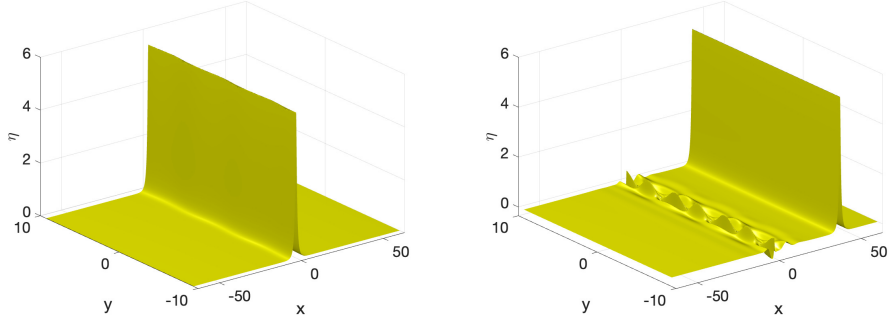


FIGURE 7. Solution to the AS system (1.4) for the initial data (2.4), on the left η for $t = 0$, on the right for $t = 20$.

is a line solitary wave of slightly higher velocity than the unperturbed wave with $c = 1.1$.

A periodic deformation of the line solitary wave similar to (2.4),

$$(2.6) \quad \eta(x, y, 0) = Q_{1.1}(x + 0.4 \cos(y)), \quad v_x(x, y, 0) = V_{1.1}(x), \quad v_y(x, y, 0) = 0,$$

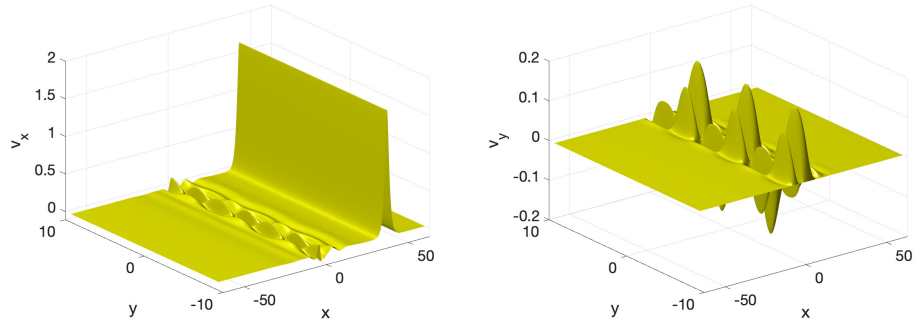


FIGURE 8. Solution to the AS system (1.4) for the initial data (2.4) for $t = 100$, on the left v_x , on the right v_y .

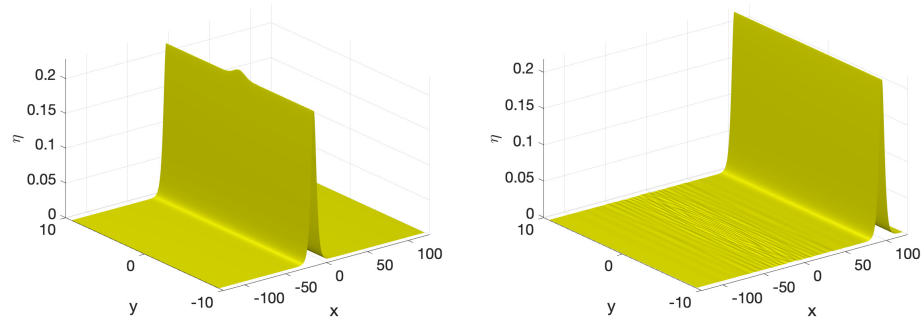


FIGURE 9. Solution to the AS system (1.4) for the initial data (2.5), on the left η for $t = 0$, on the right for $t = 100$.

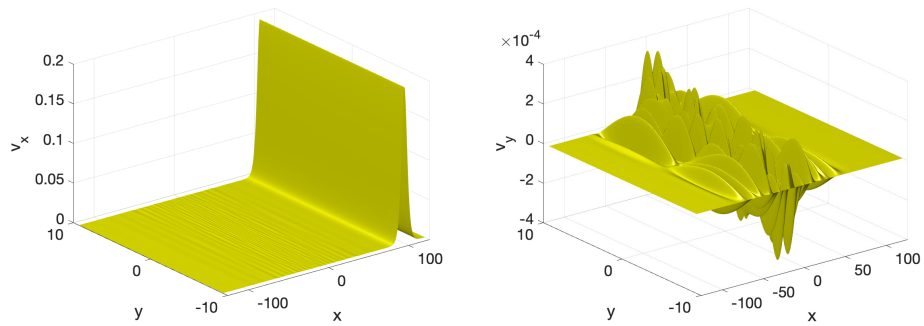


FIGURE 10. Solution to the AS system (1.4) for the initial data (2.5) for $t = 100$, on the left v_x , on the right v_y .

gives similar results as in the case $c = 2$ as can be seen in Fig. 12. The final state is once more a line solitary wave plus radiation. This is confirmed by the L^∞ norm of η in Fig. 11 on the right.

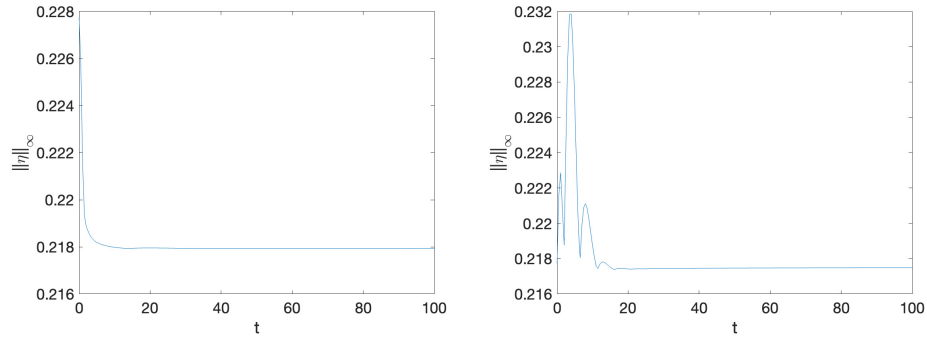


FIGURE 11. L^∞ norm of the solution to the AS system (1.4) for the initial data (2.5) on the left, on the right for the initial data (2.6).

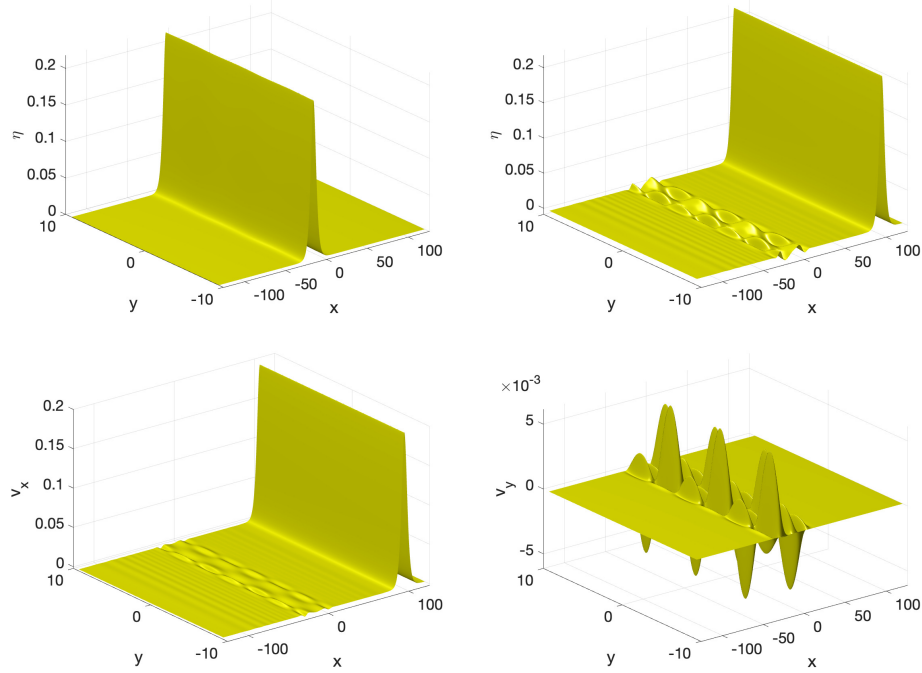


FIGURE 12. Solution to the AS system (1.4) for the initial data (2.6), in the upper row on the left η for $t = 0$, on the right for $t = 100$, in the lower row on the left v_x and on the right v_x , both for $t = 100$.

3. NON-CAVITATION CONDITION

In this section we consider initial data which violate the non-cavitation condition or come close to doing so. We first recall and expand on the case in 1D discussed in [31]. Then we discuss similar examples in 2D.

3.1. Non-cavitation condition in 1D. In [31], we have considered initial data of the form

$$\eta(x, 0) = -\exp(-x^2), \quad v(x, 0) = 0.$$

We applied the approach by Sulem, Sulem and Frisch in [44] to numerically identify singularities. It uses the fact that an essential singularity in the complex plane of the form $u \sim (z - z_j)^{\mu_j}$, $\mu_j \notin \mathbb{Z}$, with $z_j = \alpha_j - i\delta_j$ in the lower half plane ($\delta_j \geq 0$) implies for $k \rightarrow \infty$ the following asymptotic behavior of the Fourier transform (see e.g. [14], here denoted in the same way as the DFT),

$$(3.1) \quad \hat{u} \sim \sqrt{2\pi} \mu_j^{\mu_j + \frac{1}{2}} e^{-\mu_j} \frac{(-i)^{\mu_j + 1}}{k^{\mu_j + 1}} e^{-ik\alpha_j - k\delta_j}.$$

For a single such singularity with positive δ_j , the modulus of the Fourier transform decreases exponentially for large $|k|$ until $\delta_j = 0$, when this modulus has an algebraic dependence on $|k|$ for large $|k|$. The same behavior is expected in the discrete version of the Fourier transform, the DFT. In a dynamic situation, both δ_j and μ_j are expected to depend on t , and the time that δ_j vanished corresponds to the singularity hitting the real axis, i.e., to the solution forming a singularity. This will be identified by fitting the DFT coefficients to the (3.1) via some linear regression. Note that this fitting is much less reliable for the factor μ_j than for the factor δ_j since this is an algebraic correction to an exponential term. In the 1D case [31], we used 2^{18} DFT modes, but in 2D below we will be limited on the used computers to values of 2^{12} to 2^{13} . Note that if there are several singularities of the form (3.1), $j = 1, \dots, N_s$, the asymptotic expression (3.1) will involve a summation over j , but this will not be considered further (therefore we will drop the index j in the following).

For the Gaussian example, the code in [31] broke for $t \sim 4.681$ since the fitted value of δ vanished. We show the solution at the final recorded time in a close-up in Fig. 13. It can be seen that though the L^∞ norm of η gets large, a possible cusp near the origin appears to be the singular feature. The function v on the right of the same figure appears to stay regular though the fitted value of δ for v vanishes at the same time.

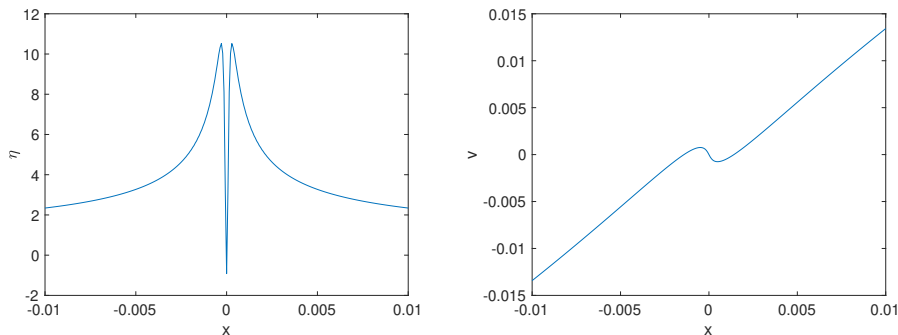


FIGURE 13. Solution to the AS system in 1D for the initial data $\eta(x, 0) = -\exp(-x^2)$, $v(x, 0) = 0$ for $t = 4.681$ in a close-up, on the left η , on the right v .

The found value for μ for the function η is negative (~ -0.85) which would indicate an L^∞ blow-up, whereas the corresponding value for v is positive ($\sim 1/3$)

which would indicate the formation of a cusp. However as mentioned, these values have to be taken with a grain of salt since they are numerically problematic as an algebraic correction to an exponential decrease. To get a better insight into the behavior of the solution, we therefore consider various norms in Fig. 14. Whereas the L^∞ norm of η appears to grow, this is not the case for various L^p norms, for instance the L^4 norm which appears to be bounded. Though numerically one cannot get close enough to a potential singularity, this is clearly an indication that there is no L^∞ blow-up to be observed in this example. The L^2 norms of the gradients in the lower row of the figure indicate, however, the blow-up of the gradient of η , but not of v . Thus it appears that there is a cusp formation in η in finite time whereas v stays regular at this time (of course we cannot rule out that higher Sobolev norms explode, it is just that v is more regular at this time than η).

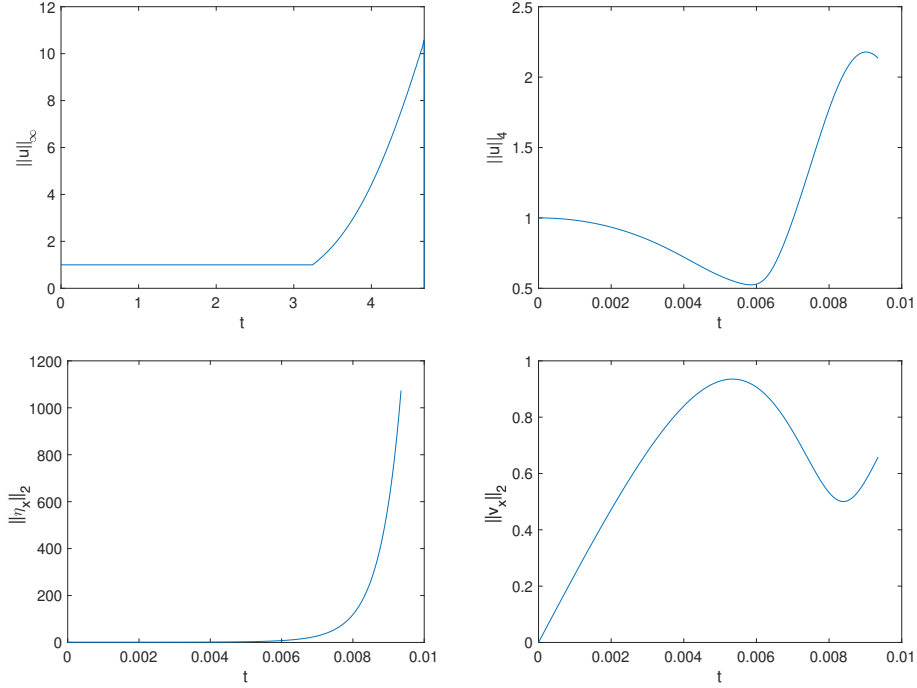


FIGURE 14. Solution to the AS system in 1D for the initial data $\eta(x, 0) = -\exp(-x^2)$, $v(x, 0) = 0$, in the upper row on the left the L^∞ norm, on the right the L^4 norm, in the lower row the L^2 norm of the gradient of η on the left (normalized to 1 for $t = 0$ as the L^4 norm) and of v on the right.

3.2. Non-cavitation condition in 2D. Concretely we look at initial data of the form (here $\kappa < 0$, $\alpha > 0$)

$$(3.2) \quad \eta(x, y, 0) = \kappa \exp(-(x^2 + \alpha y^2)), \quad v_x(x, y, 0) = v_y(x, y, 0) = 0.$$

Note that we cannot characterize potential singularities in the solutions due to a lack of resolution on the available computers.

First we study the case $\kappa = -0.9$, i.e., initial data satisfying the non-cavitation condition, but close to violating it. We use $N_x = N_y = 2^{12}$ DFT modes for $x \in 5[-\pi, \pi]$, $y \in 5[-\pi, \pi]$ and $N_t = 10^4$ time steps for the considered time interval. The solution stays smooth for all $t \leq 10$, there is as expected no indication of the appearance of a singularity. To illustrate the interesting dynamics of the solution, we first show it on the x -axis in Fig. 15 (recall the radial symmetry of the solution). For the function η shown on the left of the figure, there is a closing of the initial gap in the form of two peaks coming from the edges and eventually colliding to a central peak of high elevation, that then leads to another valley before recombining. The velocity v_x on the right of the same figure shows a similar agitated behavior.

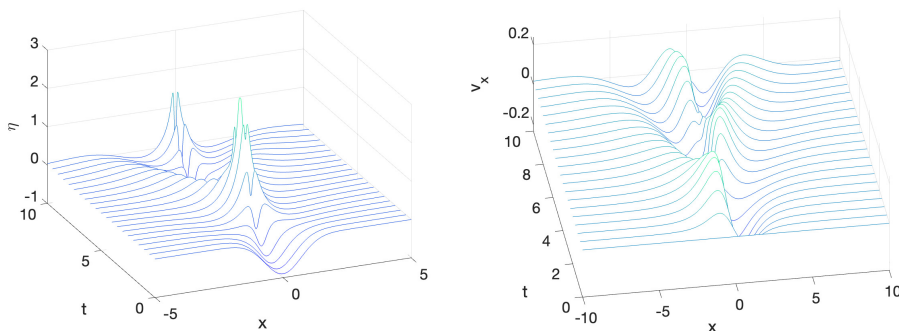


FIGURE 15. Solution to the AS system (1.4) for the initial data (3.2) with $\kappa = -0.9$ and $\alpha = 1$ on the x -axis, on the left η , on the right v_x .

To illustrate the 2D situation, we show the solution η for several values of time in Fig. 16. It is clearly visible that the peak for $t = 4$ is almost cusp-like, but then the solution forms an annular structure and a pronounced minimum appears inside the former peak.

The corresponding plots for v_x can be seen in Fig. 17. The solution appears to be always smooth though strong gradients appear. Note that the solution is always well resolved both in space and in time. The plots for v_y are very similar, just rotated by 90 degrees, and are therefore not shown.

The situation is different if the non-cavitation condition is not satisfied for the initial data, for instance for initial data of the form (3.2) with $\kappa = -1$, $\alpha = 1$ where there is one point with $\eta(x, y, 0) = 0$. We consider $N_x = N_y = 2^{12}$ DFT modes for $x \in 3[\pi, \pi]$ and $x \in 3[\pi, \pi]$. Nonetheless we find in the case $\kappa = -1$, $\alpha = 1$ that the code breaks for $t = 4.0857$ since the fitting of the DFT coefficients on the k_x axis leads to a vanishing δ in (3.1) indicating that a singularity appears on the x -axis. The fitted value for μ is 0.604, i.e., compatible with a cusp, but as we mentioned we do not have the needed numerical resolution to make a precise statement. We can only report that there is an indication of a singularity which needs to be checked on more powerful computers. Note that the same values of the fitted parameters are obtained on the y -axis. This would indicate the formation of a cusp for η of the form

$$(3.3) \quad \eta \sim (x^2 + y^2)^{\mu/2}$$

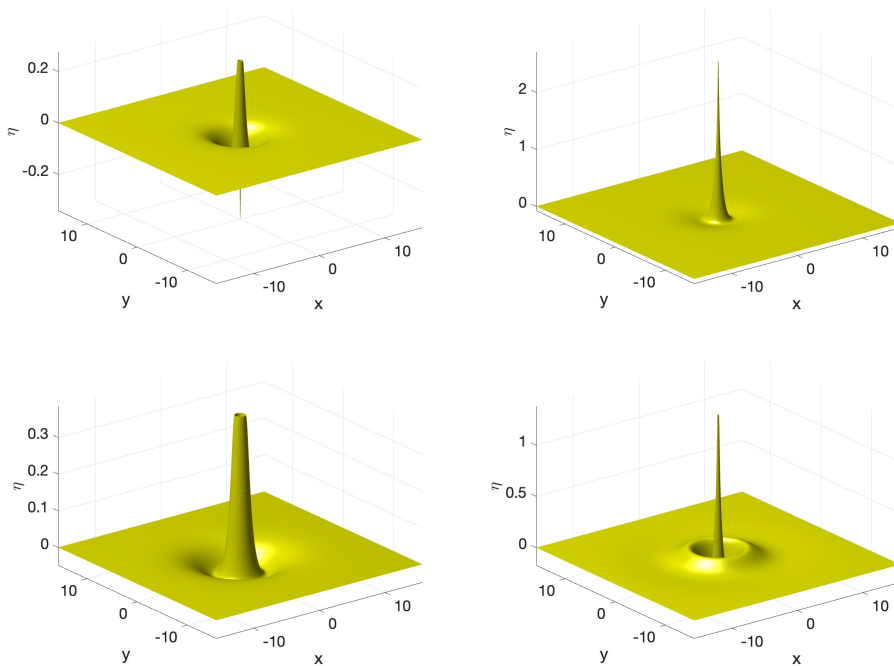


FIGURE 16. Solution η to the AS system (1.4) for the initial data (3.2) with $\kappa = -0.9$ and $\alpha = 1$, in the upper row on the left for $t = 2.5$, on the right for $t = 4$, in the lower row on the left for $t = 5.1$ and on the right for $t = 10$.

at the critical time.

Note further that the fitted values of the DFT coefficients for v_x and v_y appear to indicate that they are still regular at the critical time for η . We show the solutions at the final recorded time in Fig. 18. The behavior of η near the origin is complicated, a strong peak with a caldera.

It appears best to visualize the behavior of the solution on the x -axis which is done in Fig. 19. It can be seen that the initial depression for η is closed by two peaked maxima that are approaching each other, but that a gap remains in between these two peaks. The velocity v_x is seen in the lower row of the same figure. It seems to develop a cusp near the strongly peaked minimum of η .

As in the 1D case, we explore the possibly singular behavior via certain norms of the solution. In Fig. 20, the L^∞ norm of η appears to grow as can be seen on the left of the upper row. However as in the 1D case, a possible singularity only appears as a cusp at the minimum of the solution. This is confirmed by the L^2 norm of η (higher L^p norms are very similar) on the right. The L^2 norm of the x -derivative of η can be seen in the lower row. It appears to grow, but we clearly do not have the needed resolution to reach the potential cusp singularity. The corresponding norm for v_x does not indicate any singularity formation at the considered times.

For completeness we consider also a situation without radial symmetry, initial data of the form (3.2) with $\kappa = -1$ and $\alpha = 0.5$. We use the same computational

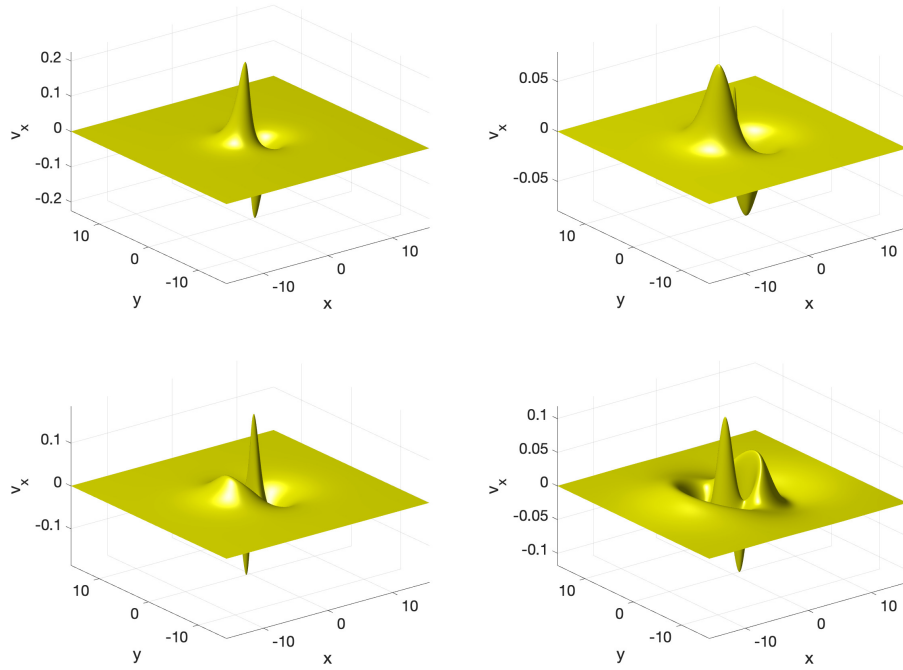


FIGURE 17. Solution v_x to the AS system (1.4) for the initial data (3.2) with $\kappa = -0.9$ and $\alpha = 1$, in the upper row on the left for $t = 2.5$, on the right for $t = 4$, in the lower row on the left for $t = 5.1$ and on the right for $t = 10$.

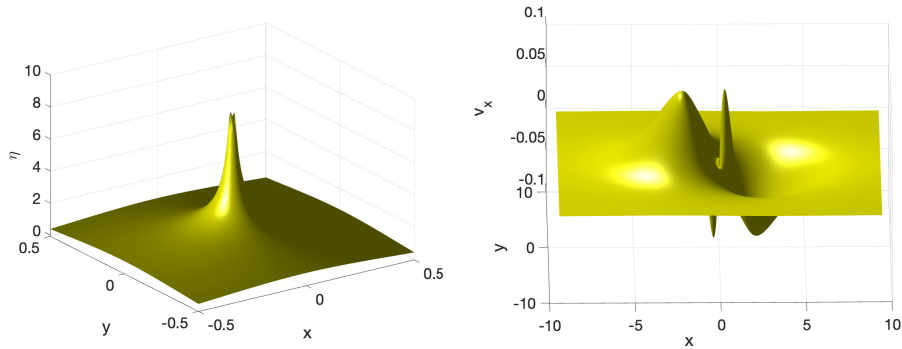


FIGURE 18. Solution to the AS system (1.4) for the initial data (3.2) with $\kappa = -\alpha = -1$, on the left η for $t = 4.0857$, on the right v_x at the same time.

domain as above, but $N_x = 2^{13}$, $N_y = 2^{11}$ DFT modes. The code breaks for $t = 4.0857$ since the fitted δ on the k_x -axis vanishes. We show the solution at the final time in Fig. 21.

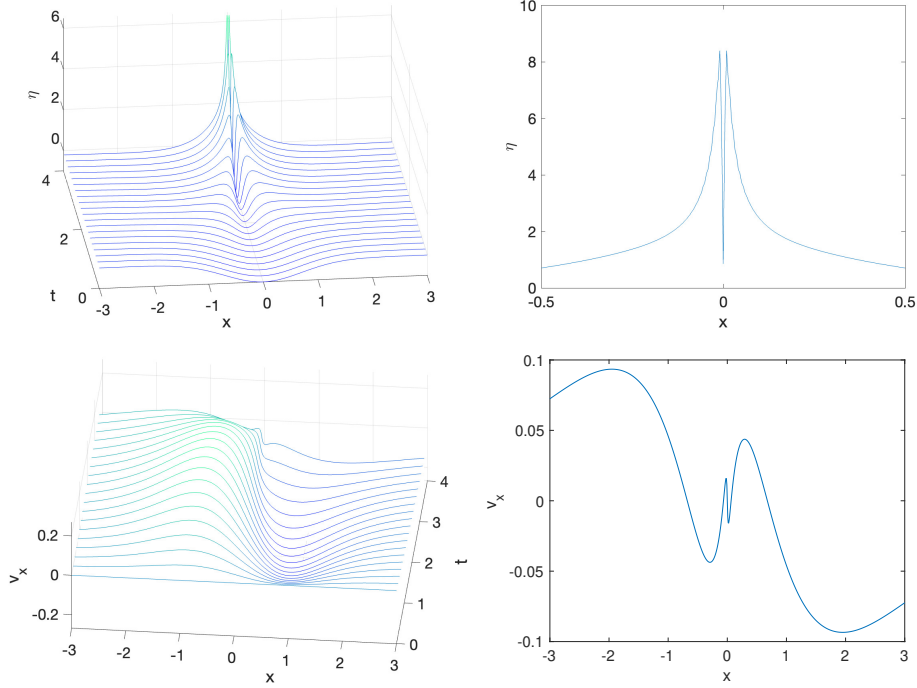


FIGURE 19. Solution to the AS system (1.4) for the initial data (3.2) with $\kappa = -\alpha = -1$ on the x -axis, in the upper row on the left in dependence of time, on the right at the critical time in a close-up, in the lower row on the left v_x and on the right a close-up at the critical time.

The corresponding fitted value for $\mu \sim -.07$ is even negative, but as in the 1D case this is not reliable. Therefore we show in Fig. 22 some norms of the solution. The L^∞ norm of η grows as in the radially symmetric case, but the L^2 norm stays finite. The L^2 norm of the x -derivative of η grows, but more slowly than in 1D which once more indicates that we lack resolution to get closer to the potential singularity. The L^2 norm of the x -derivative of v_x stays finite for the studied times.

4. LOCALISED INITIAL DATA

In this section we study the time evolution of localized initial data of the form (3.2) with positive κ . As in the study of the transverse stability of the line solitary waves, no stable structures localized in two dimensions are observed.

First we look at initial data with a small positive elevation, say $\kappa = 1$ in (3.2). The same numerical parameters as in the previous section are applied. In Fig. 23 we show the global minimum of the solution η and its L^∞ norm in dependence of time. It can be seen that an annular structure forms near the original maximum, but that the observed minimum reaches only values of the order of -0.5 before a new peak is formed. Thus one observes a similar dynamics as in the previous

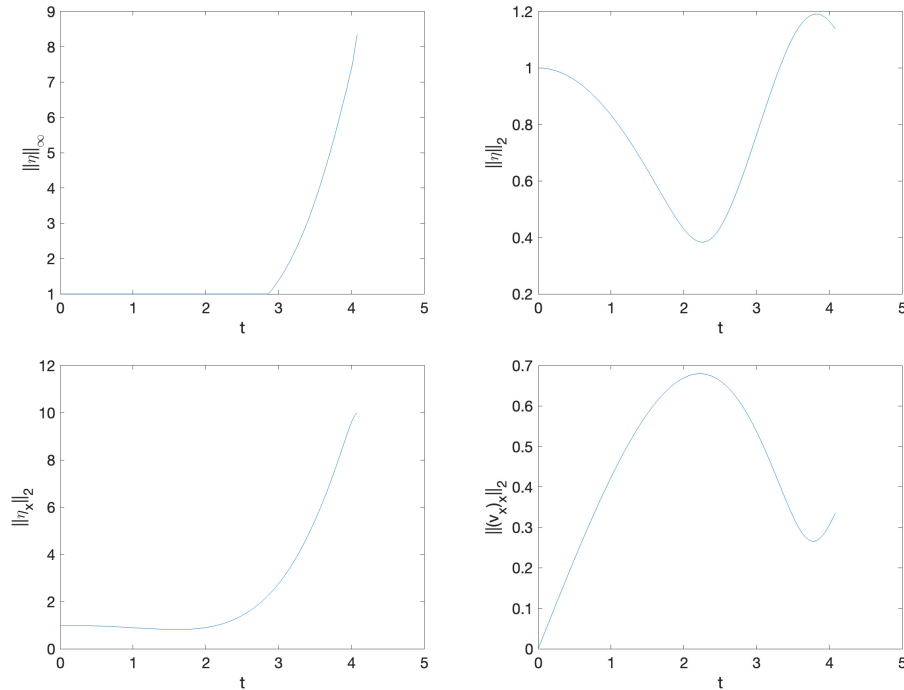


FIGURE 20. Various norms of the solution to the AS system (1.4) for the initial data (3.2) with $\kappa = -\alpha = -1$, in the upper row the L^∞ and the L^2 norm of η (normalized to 1 at $t = 0$), in the lower row the L^2 norms of the x -derivative of η (normalized to 1 at $t = 0$) and of v_x .

section. There is no indication of a stable structure emerging from these initial conditions.

This behavior of the solution can as before be best observed on the x -axis since the solution will be once more radially symmetric, see Fig. 24. The initial hump for η on the axis spreads overall, but several oscillations between annular structures and peaks can be observed. The corresponding plot for v_x on the right of the same figure shows a similar behavior starting with the trivial initial condition.

The situation becomes more agitated if initial data of larger norm are considered, for instance $\kappa = 10$ in (3.2). The time evolution of the potential on the x -axis can be seen in Fig. 25. The initial peak leads to an annular structure which develops a hole that approaches the ground to the order of -0.993 , see the lower row of the same figure on the right. It is at this point that the dynamics of the last section for near cavitation initial data takes over which is why we stop the time evolution shortly afterwards. As can be seen on the right of the lower row of the figure for the L^∞ norm, the near cavitation leads to the formation of a peak as discussed in the previous section.

To get a better understanding of the solution in the 2D setting, i.e., ignoring the radial symmetry, we show the solution η at several times in Fig. 26.

The corresponding plots for v_x can be seen in Fig. 27.

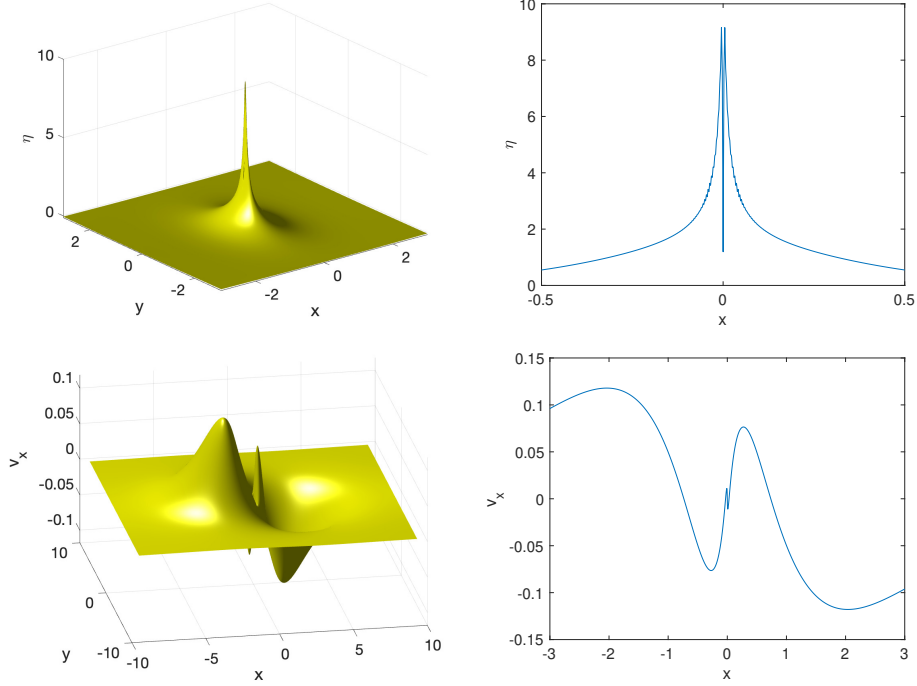


FIGURE 21. Solution to the AS system (1.4) for the initial data (3.2) with $\kappa = -1$ and $\alpha=0.5$. In the upper row on the left the solution η at the critical time, on the right a close-up of the solution on the x -axis. In the lower row the solution v_x at the critical time on the left and on the right a close-up on the x -axis.

5. DISPERSIVE SHOCK WAVES

It is well known that the solutions to nonlinear dispersive PDEs can have zones of rapid modulated oscillations near shocks of solutions for the same initial data to the corresponding dispersionless equations. These zones are called *dispersive shock waves* (DSWs). A convenient way to study DSWs is to consider initial data slowly varying on length scales of order $1/\varepsilon$ where $\varepsilon \ll 1$ for times of order $1/\varepsilon$. This can be addressed by a rescaling of both time and spatial variable with ε . In an abuse of notation (we keep the same symbols as before in order to avoid cluttered notation) we get for (1.4)

$$(5.1) \quad \begin{cases} \eta_t + \nabla \cdot \mathbf{v} + [\nabla \cdot (\eta \mathbf{v})] = 0 \\ \mathbf{v}_t + \nabla \eta + [\frac{1}{2} \nabla |\mathbf{v}|^2 - \varepsilon \Delta \mathbf{v}_t] = 0. \end{cases}$$

The formal limit $\varepsilon \rightarrow 0$ leads to a Saint-Venant system expected to have shock solutions,

$$(5.2) \quad \begin{cases} \eta_t + \nabla \cdot \mathbf{v} + [\nabla \cdot (\eta \mathbf{v})] = 0 \\ \mathbf{v}_t + \nabla \eta + [\frac{1}{2} \nabla |\mathbf{v}|^2] = 0. \end{cases}$$

To illustrate the behavior of the solutions for small values of ε , we consider once more Gaussian initial data for $\varepsilon = 10^{-2}$. The solution for $t = 5$ is shown in Fig. 28.

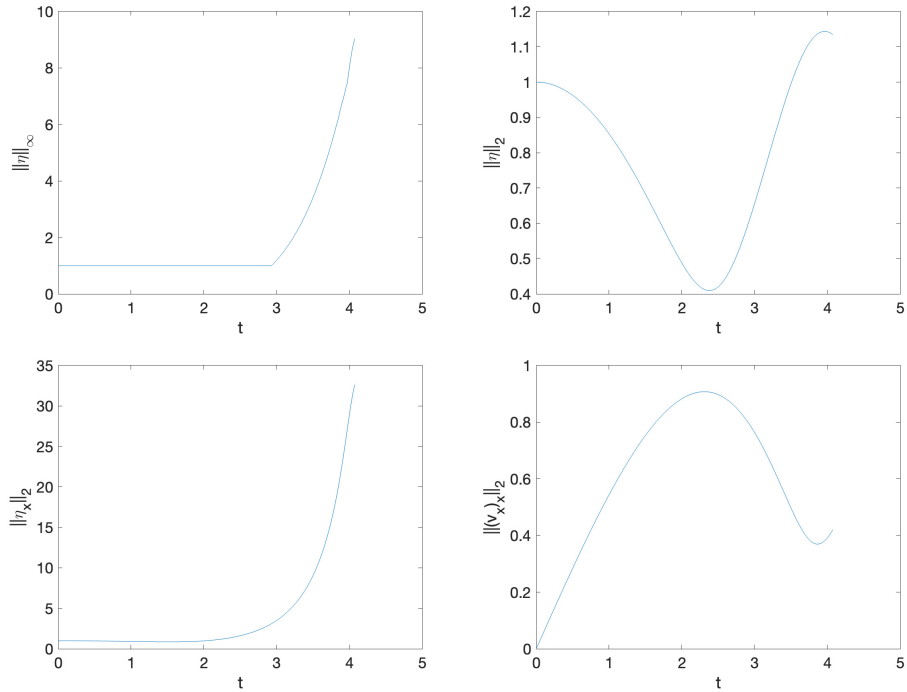


FIGURE 22. Various norms of the solution to the AS system (1.4) for the initial data (3.2) with $\kappa = -1$ and $\alpha = 0.5$, in the upper row the L^∞ and the L^2 norm of η (normalized to 1 at $t = 0$), in the lower row the L^2 norms of the x -derivative of η (normalized to 1 at $t = 0$) and of v_x .

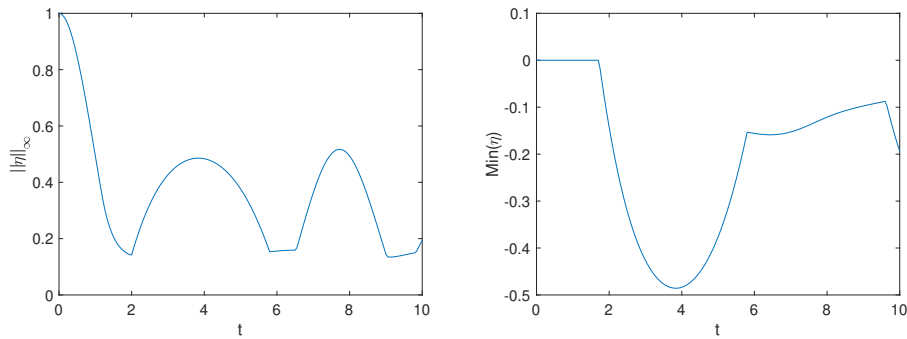


FIGURE 23. Solution to the AS system (1.4) for the initial data (3.2) with $\kappa = \alpha = 1$, on the left the L^∞ norm of η , on the right its global minimum, both in dependence of time.

It can be seen that the time evolution is similar to what was shown in the previous section, an initial peak develops into some annular structure for η . But the small

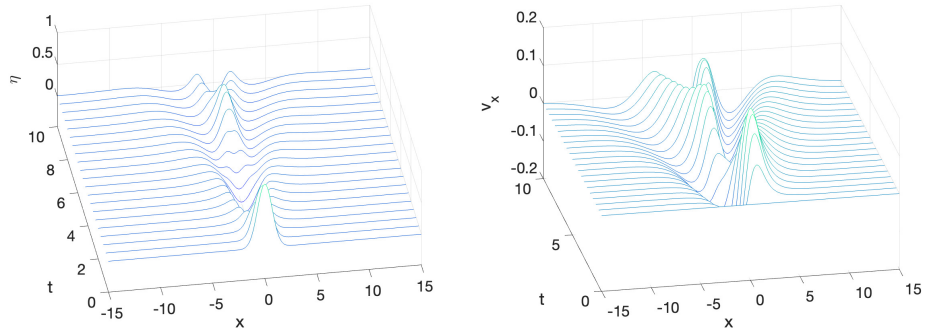


FIGURE 24. Solution to the AS system (1.4) for the initial data (3.2) with $\kappa = \alpha = 1$ on the x -axis in dependence of time, on the left η , on the right v_x .

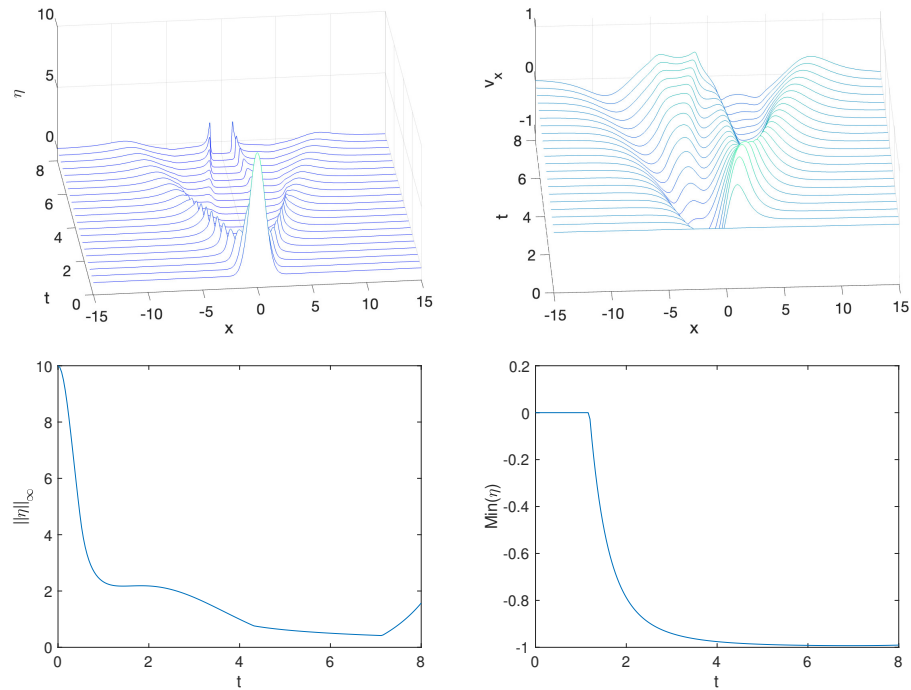


FIGURE 25. Solution to the AS system (1.4) for the initial data (3.2) with $\kappa = 10$, $\alpha = 1$ on the x -axis in dependence of time in the upper row, on the left η , on the right v_x , in the lower row the L^∞ norm of the solution on the left and the global minimum on the right.

value ε leads to very strong gradients in an almost tubular structure, and similarly for v_x .

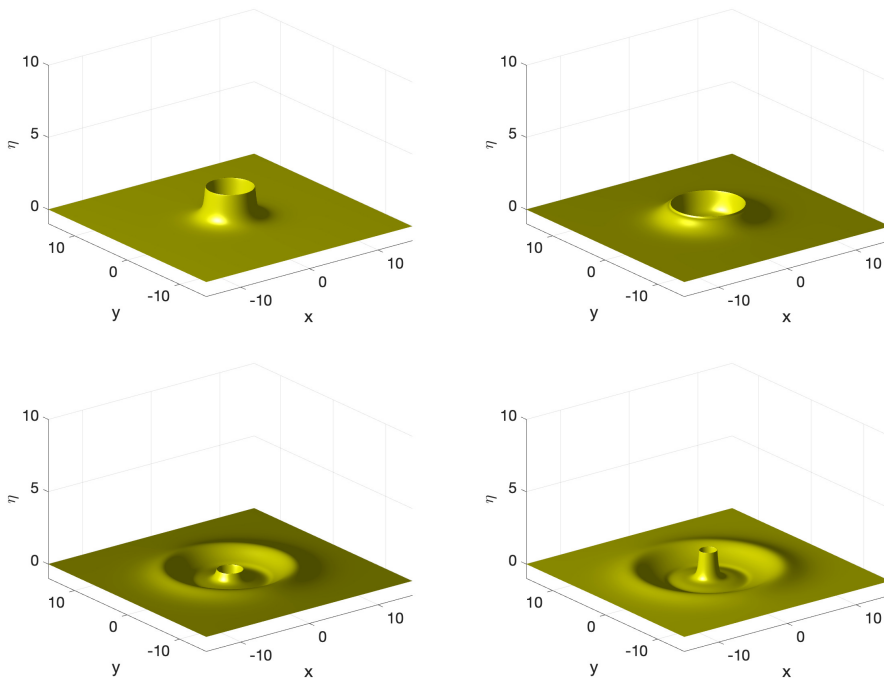


FIGURE 26. Solution η to the AS system (1.4) for the initial data (3.2) with $\kappa = 10$, $\alpha = 1$ for several values of time, in the upper row for $t = 2$ and $t = 4$, in the lower row for $t = 6.92$ (time close to the minimal value) and $t = 8$.

However there are small oscillation on what appears to be a steep front in Fig. 28. To illustrate this, we show the potentials in Fig. 28 on the axis together with a close-up of the oscillatory zone in Fig. 29. It can be seen that there are modulated oscillations near the strong gradients.

6. CONCLUSION

In this paper we have presented a numerical study of the 2D Amick-Schonbek system (1.4). Numerical evidence for the transverse stability of line solitary waves was presented as well as for the absence of stable lump solitary waves, i.e., for solitary waves localised in both spatial dimensions. It was shown that solutions to the system can exhibit zones of rapid modulated oscillations known as dispersive shock waves. It was argued that initial data not satisfying the non-cavitation condition lead to the formation of cusps in finite time. A precise characterization of these cusp was not possible due to a local of numerical resolution. This will be the subject of further research.

Similar numerical studies will be performed for the Boussinesq system integrable in 1D and numerically studied in [32]. The results are to be compared to other equations appearing in the context of water waves as the Serre-Green-Naghdi equations [23, 24, 43]. The goal is to expand the study of [22] to the questions addressed in the present paper. This will be the subject of future work.

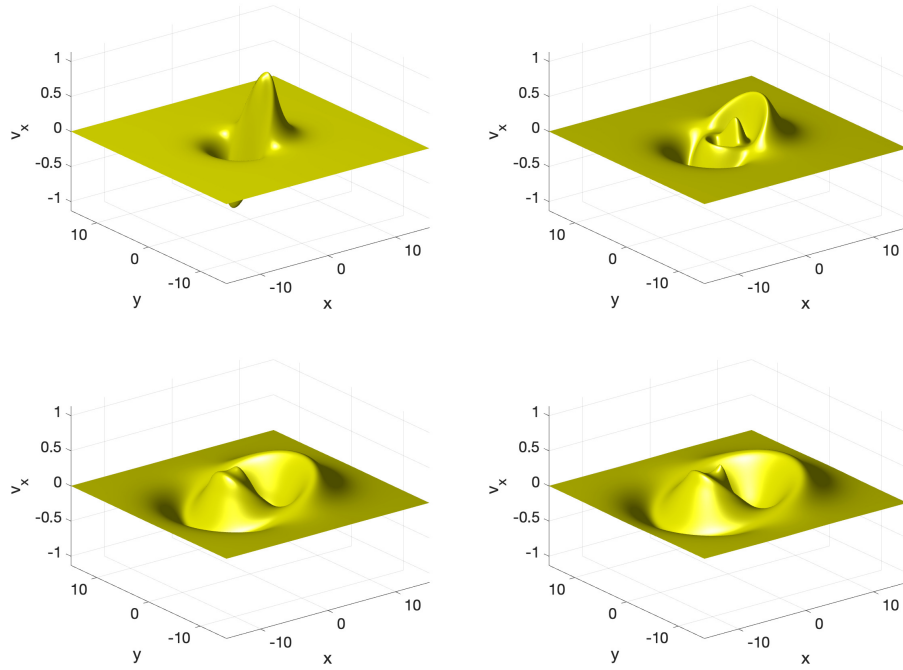


FIGURE 27. Solution v_x to the AS system (1.4) for the initial data (3.2) with $\kappa = 10$, $\alpha = 1$ for several values of time, in the upper row for $t = 2$ and $t = 4$, in the lower row for $t = 6.92$ and $t = 8$.

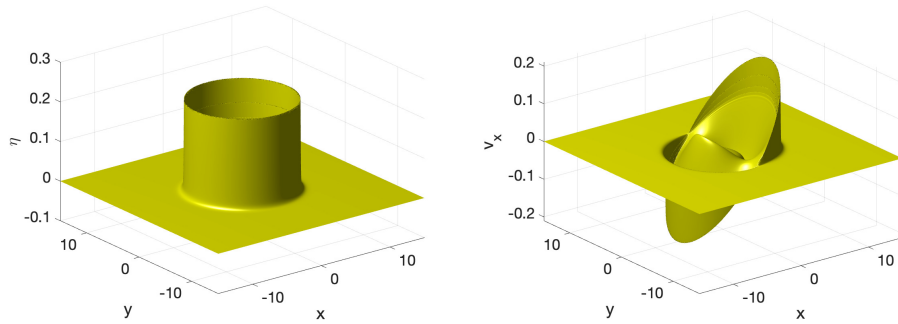


FIGURE 28. Solution to the AS system (5.1) for the initial data (3.2) with $\kappa = \alpha = 1$ and $\varepsilon = 10^{-2}$ for $t = 5$, on the left η , on the right v_x .

Acknowledgements. The work of the first author was partially supported by the ANR project ANR-17-EURE-0002 EIPHI.

Both authors were partially supported by the ANR project ISAAC-ANR-23-CE40-0015-01.

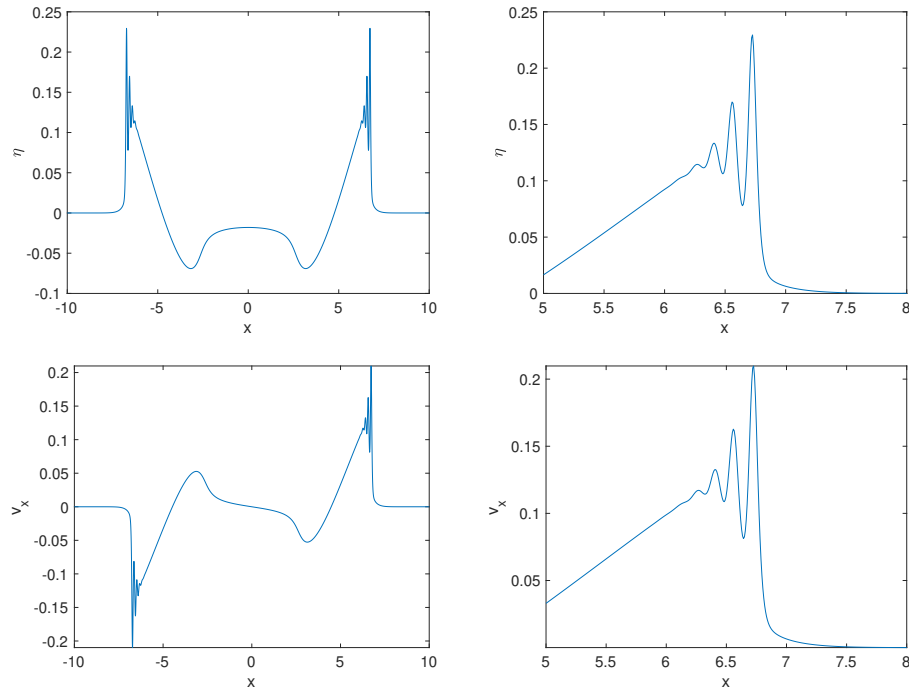


FIGURE 29. Solution to the AS system (5.1) for the initial data (3.2) with $\kappa = \alpha = 1$ and $\varepsilon = 10^{-2}$ for $t = 5$ on the x -axis, in the upper row η , in the lower v_x , both with a close-up of the oscillatory zone on the right.

REFERENCES

1. K. ADAMY, *Existence of solutions for a Boussinesq system on the half line and on a finite interval*, Discrete Cont. Dyn. Systems **29** (1) (2011), 25-49.
2. C.J. AMICK, *Regularity and uniqueness of solutions for the Boussinesq system of equations*, J. Differential Eq. **54** (1) (1984), 231-247.
3. D. ANTONOPOULOS AND V. DOUGALIS, *Numerical solution of the "classical" Boussinesq system*, Math. Comp. Simul. **82** (2012), 984-1007.
4. D. ANTONOPOULOS AND V. DOUGALIS, *Error bestimates for Galerkin approximations of the "classical" Boussinesq system*, Math. Comp. **82** (2013), no. 282, 689-717.
5. D.C. ANTONOPOULOS, V. A. DOUGALIS AND D. E. MITISOTAKIS, *Galerkin approximations of periodic solutions of Boussinesq systems*, Bull. Greek Math. Soc. **57** (2010), 13-30.
6. H. BERESTYCKI AND P.-L. LIONS, *Nonlinear scalar field equation I*, Arch. Rat. Mech. Anal. **32** (1983), 313-346.
7. L. BRUDVIK-LINDNER, D. MITSOTAKIS AND A. E. TZAVARAS, *Oscillatory and regularized shock waves for a dissipative Peregrine-Boussinesq system*, IMA Journal of Applied Mathematics (2023) <https://doi.org/10.1093/imamat/hxad030>
8. J. L. BONA, T. COLIN AND D. LANNES, *Long-wave approximation for water waves*, Arch. Ration. Mech. Anal. **178**, (2005), 373-410.
9. J. L. BONA, M. CHEN AND J.-C. SAUT, *Boussinesq equations and other systems for small-amplitude long waves in nonlinear dispersive media I : Derivation and the linear theory*, J. Nonlinear Sci. **12** (2002), 283-318.

10. J. L. BONA, M. CHEN AND J.-C. SAUT, *Boussinesq equations and other systems for small-amplitude long waves in nonlinear dispersive media. II : The nonlinear theory*, Nonlinearity **17** (2004) 925-952.
11. J. BOUSSINESQ, *Théorie des ondes et des remous qui se propagent le long d'un canal rectangulaire horizontal, en communiquant au liquide contenu dans ce canal des vitesses sensiblement pareilles de la surface au fond*, J. Math. Pures Appl. **7** (2) (1872), 55-108.
12. L.F.J. BROER, *Approximate equations for long water waves*, Appl. Sci. Res. **31** (1975), 377-395.
13. C. BURTEA, *New long time existence results for a class of Boussinesq-type systems*, J. Math. Pures Appl. **106** (2) (2016), 203-236.
14. G. CARRIER AND M. K. C. PEARSON, *Functions of a Complex Variable, Theory and Technique*, Society for Industrial and Applied Mathematics (SIAM), Philadelphia, PA, 2005.
15. MIN CHEN, *Solitary-wave and multi-pulsed traveling-wave solutions of Boussinesq systems*, Appl. Anal. **75** (1-2) (2000), 213-240.
16. W. CRAIG AND C. SULEM, *Numerical simulation of gravity waves*, J. Comput. Phys. **108** (1993), 73-83.
17. O. DARRIGOL, *Worlds of flow. A hydrodynamics from the Bernoullis to Prandtl*, Oxford University Press 2005.
18. O. DARRIGOL, *The Spirited Horse, the Engineer, and the Mathematician : Water Waves in Nineteenth-Century Hydrodynamics*, Arch. Hist. Exact Sci. **58** (2003), 21-95.
19. O. DARRIGOL, *Joseph Boussinesq's legacy in fluid mechanics*, C.R. mechanics **345** (2017), 427-445.
20. M.W. DINGEMANS, *Water wave propagation over uneven bottoms. Part 2- Non-linear Wave Propagation*, Advances Series on Ocean Engineering-Volume 13. World Scientific, (2000).
21. V. Duchêne, C. Klein, *Numerical study of the Serre-Green-Naghdi equations and a fully dispersive counterpart*, Discr. & Cont. Dyn. Syst. B, **27**(10), 5905-593 (2021) doi: 10.3934/dcdsb.2021300
22. S. Gavriljuk, C. Klein, *Numerical study of the Serre-Green-Naghdi equations in 2D*, Nonlinearity **37** 045014 DOI 10.1088/1361-6544/ad2eb8
23. A. E. Green, N. Laws and P. M. Naghdi, *On the theory of water waves*, Proc. R. Soc. Lond. A **338** (1974), 43-55.
24. A. E. Green and P. M. Naghdi, *A derivation of equations for wave propagation in water of variable depth*, J. Fluid Mech. **78** (1976), 237-246.
25. A.S. FOKAS, *A unified transform method for solving linear and certain nonlinear PDE's*, Proc. Roy. Soc. A **453** (1997), 1411-1443.
26. A.S. FOKAS AND B. PELLONI, *Boundary value problems for Boussinesq type systems*, Analysis and Geometry **8** (2005), 59-96.
27. G. KOUNADIS, D.C. ANTONOPOULOS, V.A. DOUGALIS, *Galerkin finite element methods for the numerical solution of two classical Boussinesq type systems over variable bottom*, Wave Motion **102** (2021), 102715.
28. M.D. GROVES, *Hamiltonian long-wave approximations for water waves in a uniform channel*, in Nonlinear Dispersive Wave Systems, Lokenath Debnath Ed. World Scientific (1992), 99-125.
29. C.M. JOHNSTON, C.T. GARTMAN AND D. MANTZAVINOS, *The linearized classical Boussinesq system on the half-line*, Studies in Applied Math. **146** (2021), 635-657
30. C. KLEIN AND K. ROIDOT, *Numerical study of shock formation in the dispersionless Kadomtsev-Petviashvili equation and dispersive regularizations*, Physica D, Vol. 265, 1-25, 10.1016/j.physd.2013.09.005 (2013).
31. C. Klein, J.-C. Saut, *Numerical study of the Amick-Schonbek system*, Stud Appl Math. 2024;1-22. <https://doi.org/10.1111/sapm.12691>
32. C. Klein, J.-C. Saut, *On the Kaup-Broer-Kupershmidt systems*, <https://doi.org/10.48550/arXiv.2402.17576>
33. C. KLEIN AND J.-C. SAUT, *A numerical approach to blow-up issues for dispersive perturbations of Burgers' equation*, Physica D: Nonlinear Phenomena (2015), 46-65, 10.1016/j.physd.2014.12.004
34. C. KLEIN AND J.-C. SAUT, *Nonlinear dispersive equations - Inverse Scattering and PDE methods*, Applied Mathematical Sciences 209 (Springer, 2022)
35. D. LANNES, *Water waves : mathematical theory and asymptotics*, Mathematical Surveys and Monographs, vol 188 (2013), AMS, Providence.

36. B. MELINAND, *Dispersion estimates for non-homogeneous radial phases : an application to weakly dispersive equations and water waves models*, J. Funct. Analysis **286** (2023), 110204.
37. B. MESOGNON-GIREAU, *The Cauchy problem on large time for a Boussinesq-Peregrine equation with large topography variations*, Ann. I.H. Poincaré-AN **34** (2017), 89-118.
38. L. MOLINET, R. TALHOUK AND I. ZAÏTER, *The classical Boussinesq system revisited*, Nonlinearity **34** (2) (2021), 744-775.
39. D.H. PEREGRINE, *Long waves on a beach*, J. Fluid Mech. **27** (1967), 815-827.
40. Y. SAAD, M. SCHULTZ, *GMRES: A generalized minimal residual algorithm for solving non-symmetric linear systems*, SIAM J. Sci. Stat. Comput. **7** (3), 856-869 (1986).
41. J. C. SAUT, C. WANG AND L. XU, *The Cauchy problem on large time for surface waves Boussinesq systems II*, SIAM Journal on Mathematical Analysis, **49** (4) (2017), 2321-2386.
42. M.E. SCHONBEK, *Existence of solutions to the Boussinesq system of equations*, J. Differential Eq. **42** (1981), 325-352.
43. F. Serre, *Contribution à l'étude des écoulements permanents et variables dans les canaux*, La Houille Blanche 8 (1953), 374-388.
44. C. SULEM, P. SULEM, AND H. FRISCH, *Tracing complex singularities with spectral methods*, J. Comp. Phys., 50 (1983), pp. 138-161.
45. M. H. TENG AND T. Y. WU, *Nonlinear water waves in channels of arbitrary shape*, J. Fluid Mech. **242** (1992), 211-233.
46. T. Y. WU, *A bidirectional long wave model*, Methods and Applications of Analysis. **1** (1) (1994), 108-117.
47. V.E. ZAKHAROV, *Weakly Nonlinear Waves on Surface of Ideal Depth Fluids*, Amer. Mat. Soc. Transl. Ser. 2 **182**, 167-197.

INSTITUT DE MATHÉMATIQUES DE BOURGOGNE, UMR 5584, INSTITUT UNIVERSITAIRE DE FRANCE,
UNIVERSITÉ DE BOURGOGNE EUROPE, 9 AVENUE ALAIN SAVARY, 21078 DIJON CEDEX, FRANCE
Email address: Christian.Klein@u-bourgogne.fr

LABORATOIRE DE MATHÉMATIQUES, UMR 8628, UNIVERSITÉ PARIS-SACLAY ET CNRS, 91405
ORSAY, FRANCE
Email address: jean-claude.saut@universite-paris-saclay.fr